



## Comparison of Recent Remote Sensing Data Using an Artificial Neural Network to Predict Soil Moisture by Focusing on Radiometric Indices

Miraç Kılıç<sup>1,a,\*</sup>, Recep Gündoğan<sup>2,b</sup>

<sup>1</sup>Department of Plant and Animal Production, Vocational School of Kahta, Adıyaman University, Adıyaman, Türkiye

<sup>2</sup>Department of Soil Science and Plant Nutrition, Agriculture Faculty, Harran University, Sanlıurfa, Türkiye

\*Corresponding author

### ARTICLE INFO

### ABSTRACT

#### Research Article

Received : 01/09/2022

Accepted : 29/09/2022

#### Keywords:

Multi-layer perceptron

Landsat 9

Soil moisture

Soil adjusted vegetation index

Normalized difference moisture index

Remote sensing data is widely used as a common variable for digital soil mapping estimating models. The aim of this study, quite recently made available to researchers Operational Land Imager 2 (OLI-2) have structure Landsat 9 and Landsat 8 (OLI) and Sentinel 2A (MSI) to compare the performance of soil moisture estimation in multi-layer perceptron network (MLP) artificial intelligence algorithm of image data. The working area is 886.78 km<sup>2</sup> and soil sampling was performed at 66 points for gravimetric soil moisture determination. In addition, after the satellite images were pre-processed, Soil Adjusted Vegetation Index (SAVI) and Normalized Difference Moisture Index (NDMI) were calculated. Landsat 9 (OLI-2) based SAVI and NDMI showed a moderately significant positive correlation relationship with gravimetric soil moisture ( $r_{SAVI-SM}=0.62$ ,  $r_{NDMI-SM}=0.44$ ). The relationship between Landsat 8 (OLI) ( $r_{SAVI-SM}=0.57$ ,  $r_{NDMI-SM}=0.11$ ) and Sentinel 2A (MSI) ( $r_{SAVI-SM}=0.42$ ,  $r_{NDMI-SM}=0.27$ ) based radiometric indices and soil moisture was lower than Landsat 9 (OLI-2). RMSE values of MLP models were found to be respectively 0.79, 1.16 and 1.17 for Landsat 9 (OLI-2), Landsat 8 (OLI) and Sentinel 2A (MSI). Our results showed that with an Operational Land Imager (OLI-2) and near and short-wave infrared wavelengths improvements to multispectral imaging have improved soil moisture estimation success.

[mirackilic@adiyaman.edu.tr](mailto:mirackilic@adiyaman.edu.tr)

<https://orcid.org/0000-0001-8026-5540>

[rgundogan@harran.edu.tr](mailto:rgundogan@harran.edu.tr)

<https://orcid.org/0000-0001-8877-1130>



This work is licensed under Creative Commons Attribution 4.0 International License

## Introduction

Soil moisture is an important component of the hydrological cycle, which regulates surface runoff, crop production and evaporation. (Kraft et al., 2022). In addition, early water deficiency conditions, yield estimation and food security; is a physical property of land that is taken into account in practices such as policy making, decision-making and crop planning (Carlson, 2007; Sadri et al., 2020) Therefore, soil moisture modelling and monitoring is of increasing interest. Monitoring of spatial and temporal variations of soil moisture, it is a prerequisite for both the sustainability of crop production and the development of precision agriculture and food security. (Lloret et al., 2021; Mukwada et al., 2021; Oliveira et al., 2021). Surface soil moisture; although usually the top of the soil layer refers to the water content of ~5-15 cm; plays an important role in biochemical and physiological processes. Accurate information about spatial and temporal variations of surface soil moisture is

crucial for policy-making and soil-water management (O'Connell et al., 2018; L. Wang & Qu, 2009).

Optical satellite sensors are very useful data sources for mapping surface moisture. Besides this, active microwave sensors are also a remote sensing data source for soil moisture. (Wang, 2019). However, optical satellite sensors stand out for their large data archive, as well as having high spatial resolution. The best example of this is Landsat TM's data archive since 1972 (USGS, 2013). Another advantage of optical satellite sensors is that they detect in many regions of the electromagnetic spectrum. Based on the fact that moisture content affects soil electro-magnetic radiation (EMR); using visible and infrared wavelengths, there are studies in which the topsoil moisture content is successfully estimated (Abowarda et al., 2021; Pittaki-Chrysodonta et al., 2018). Soil moisture based on spectral characteristics, Soil Adjusted Vegetation Index (SAVI) can be detected using electromagnetic radiation differences in the near Infrared (NIR) and red spectrum band (Amani et

al., 2016; Babaeian et al., 2019). Another method for detecting soil moisture using satellite data is Normalized Difference Moisture Index (NDMI), which takes into account reflection on the NIR and Short-Wave Infrared spectrum (Bidgoli et al., 2020). With this approach, the moisture content can be estimated by taking advantage of the MODIS data NIR and red reflection differences. However, due to its low spatial resolution, it is disadvantageous compared to the Sentinel and Landsat satellites. (Zhang et al., 2019). Instead of a single band of the existing remote sensing data set, the remote sensing indices were used as a covariate in the multilayer perceptron (MLP) model.

The use of artificial intelligence algorithms in soil moisture estimation is gradually increasing. In these researches, prediction algorithms or common variables differ. Many researchers, such as Zounemat-Kermani et al. (2022) have predicted soil moisture with the MLP, using meteorological data as a covariate. Data supply can create a constraint in soil moisture forecasting using meteorological data. Because the prevalence of meteorological stations where data to be used for soil moisture estimation can be obtained is not yet at the desired level. In this respect, remote sensing data is a very useful alternative. Chaudhary et al. (2022), Sentinel-1 conducted soil moisture estimation with radar backscatter data and 12 advanced machine learning algorithms and he reported that MLP is a successful model.

Studies of soil moisture estimation with Landsat 9, which recently became available to researchers, are not yet at an adequate level. NASA-USGS, which aims to ensure the continuity of land observations by developing technical capabilities, the latest member of the joint mission with Landsat 9, Operational Land Imager 2 (OLI-2) has presented improvements for multispectral imaging at near- and short-wave infrared wavelengths. (Masek et al., 2020) In addition; Sentinel 2 has been made available free of charge by ESA for environmental monitoring purposes and has been used in many scientific researches. This study aims to evaluate the effect of Landsat 9 OLI-2, Landsat 8 OLI and Sentinel 2 MSI radiometric indices on soil moisture estimation success in MLP.

## Material Method

### Study Area

The study area located in the south of Besni district of Adıyaman province (37° 40' 7" - 38° 10' 5" East and 37° 25' 0" - 37° 40' 5" North) covers an area of 886.78 km<sup>2</sup> where intensive agricultural production is carried out. Within the working area; Keysun, Kızılın and Sahantil plains are located and to the south, Tavaş and Çövenek waters merge to the south to the Göksu river, and to the north are the Değirmen streams. (Ortaç, 2020). The average annual temperature is 17.7°C, the average annual rainfall is 636 mm (Mevbis, 2022). The study area consists of geological units of mesozoic-aged limestone, marl and schist. There are also locally various ophiolitic groups and alluviums in valley floors and stream circles. Its geomorphological structure is mainly a karst plateau torn apart by streams. (Yıldırım, 2004).

### Soil Sampling and Analysis Method

With a total width of 886.78 km<sup>2</sup>, the working area is divided into 4 km x 4 km grids; soil samples were collected at 66 points and a depth of 0–20 cm from the approximate center of each grid. Also; taking into account lithological characters, vegetation and topography, both to ensure an even distribution of samples based on these characteristics and to increase model success 4 intersample was performed at intervals of 100 m, 500 m, 750 m and 1250 m between the sample points. (Figure 1). Soil samples taken from the field were made air dry and passed through a 2 mm sieve. Then, to determine the spatial distribution of soil moisture content, in the creation of the mathematical function, the percentage of moisture in the samples taken in the field study for reference is calculated by gravimetric method to equation 1 (Tüzüner, 1990).

$$\text{Soil moisture (\%)} = \frac{(A-B) \times 100}{E} \tag{1}$$

In the above equation, A, B and E are respectively; tare wet soil, tare dry soil, and oven dry soil weigh.

Table 1. Image bands used to calculate remote sensing indices (Cerasoli et al., 2018; USGS, 2019)

Landsat 8 OLI		Landsat 9 OLI-2			Sentinel 2A MSI		
Band	Spectral Region Wavelength (nm)	Band	Spectral Region Wavelength (nm)	Band	Spectral Region Wavelength (nm)	Band	Spectral Region Wavelength (nm)
4	Red 630-680	4	Red 640-670	4	Red 650-580		
5	NIR 845-885	5	NIR 850-880	8	NIR 785-899		
6	SWIR 1560-1660	6	SWIR 1570-1650	11	SWIR 1565-1655		

Table 2. Performance (error) criteria for models

Abbreviation	Error Metrics	Equation	Reference
RMSE	Root Mean Square Error	$\sqrt{\frac{1}{n} \sum_{t=1}^n [(\hat{Z}(x_i) - Z(x_i))]^2}$	(Somaratne et al., 2005)
MAE	Mean Absolute Error	$\frac{1}{n} \sum_{i=1}^n  \hat{Z}(x_i) - Z(x_i) $	(Isaaks & Mohan, 1989)

Table 3. Descriptive statistics for soil moisture contents in workspace-all, training and validation datasets.

	Min. (%)	Mak. (%)	Median (%)	Mean (%)	Std. Dev (%)
Whole dataset	1.10	7.31	2.87	2.35	1.45
Training dataset	1.10	7.21	2.35	2.82	1.39
Test dataset	1.10	7.31	2.67	3.01	1.61

Table 4. Optimum MLP architectural parameters to estimate soil moisture

Model	Numbers of		Activation Function	R <sup>2</sup>		RMSE		MAE	
	Neurons	Hidden Layer		Training	Test	Training	Test	Training	Test
Landsat 8	7-7	2	tansig	0.791	0.536	0.61	1.16	0.49	0.85
Landsat 9	7-7	2	tansig	0.838	0.790	0.53	0.79	0.42	0.66
Sentinel 2A	7-7	2	tansig	0.818	0.581	0.57	1.17	0.45	0.87

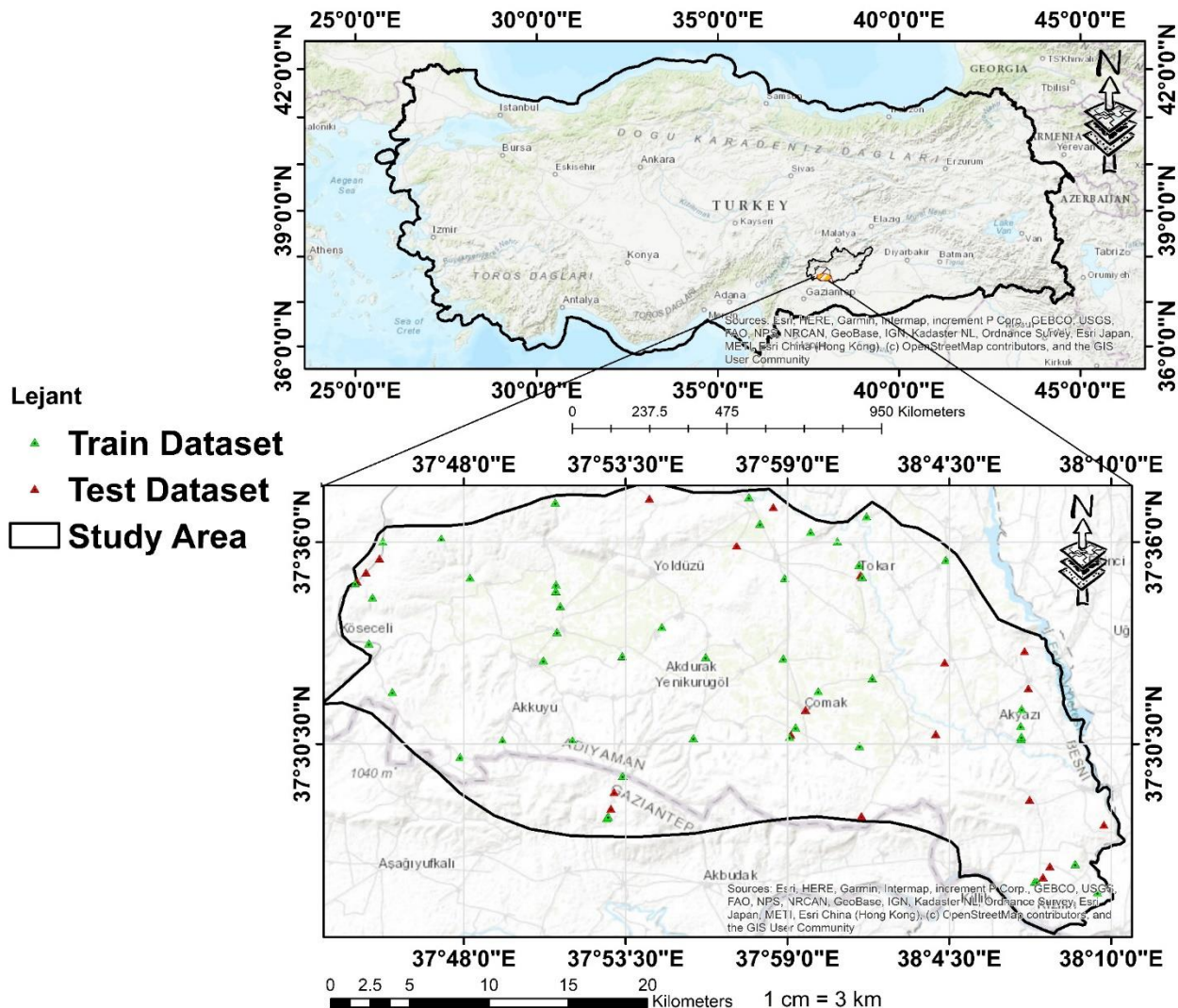


Figure 1. Geographic locations of the workspace, training, and testing dataset

**Remote Sensing Data**

Landsat 9 OLI 2 satellite imagery is available free of charge by NASA-USGS as of February 2022. In the study presented, the May 2022 images of our workspace were obtained from earthexplorer.usgs.gov. The Sentinel 2A image from the same date was obtained from the European Space Agency (ESA).

Prior to further interpretation and analysis specific pre-processing of the raw image data is required. Some of these operations are intended to correct errors during the retrieval of data. So in the first stage, radiometric correction, which is one of the pre-processing steps required for healthy

information extraction by using remote sensing images, was made. Thanks to radiometric correction, errors caused by atmospheric effects in pixel brightness values have been eliminated. Because, the signals reaching the satellite sensor are affected by many suspended particles and materials in the atmosphere, such as water vapour, aerosols and other gases, and are at pixel values causing errors (Khorram et al., 2012). First of all, bands of the upper atmosphere of the Landsat 9 (OLI-2), Landsat 8 (OLI) and Sentinel 2A MSI images, has been atmospherically corrected using the Semi-Automatic Classification

package, which works as an add-on to the QGIS software. In addition, the atmospheric correction was performed with the Dark Object Subtraction method (DOS1), which is widely used in remote sensing (Congedo, 2021; Senel, 2018). In this new dataset, Landsat 9 (OLI-2), Landsat 8 (OLI) and Sentinel 2A (MSI) NIR and SWIR (Table 1) bands were clip according to the working area boundaries.

SAVI and NDMI values were then obtained from the data subjected to image processing. To determine the index value and stress levels of vegetation in the study area, SAVI was calculated according to equation 2 given below (Casamitjana et al., 2020; Huete, 1988).

$$SAVI = \frac{(1+L) \times (NIR-Red)}{L+NIR+Red} \quad (2)$$

In the equation: NIR represents the spectral value of reflection in the near infrared band (785-899 nm); Red represents the reflective value of the red band (650-680 nm) and L represents the brightness correction factor (0.5).

In the next data processing step, the value of NDMI, which is used to determine vegetation stress in relation to the level of soil moisture, is calculated according to equation 3 (Das et al., 2021).

$$NDMI = \frac{NIR-SWIR}{NIR+SWIR} \quad (3)$$

In the equation: NIR represents the spectral value of reflection in the near infrared band (785-899 nm); SWIR represents the shortwave infrared (1565-1655 nm) reflectance value.

### Modeling Approach

To create soil moisture prediction model with different remote sensing datasets, artificial neural network with multilayer perceptron forward feeding algorithm was used with input variables. The first layer of MLP is the input layer, which consists of the input variables of our model. The last layer is the output layer that consists of the output results. The layers between the input and output layers are hidden layers. Once the architecture of the MLP is created, it needs to be trained. In the presented study, Levenberg-Marquardt backpropagation training algorithm was used. Levenberg-Marquardt is a training function that optimizes weight and bias values (Figure 2). This algorithm Figure 2. Schematic diagram representing MLP network architecture

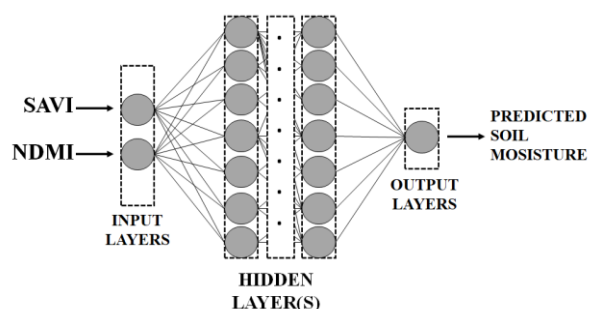


Figure 2. Schematic diagram representing MLP network architecture

is the MLP training algorithm that is widely used in digital soil mapping applications. (Dai et al., 2014; Sergeev et al., 2019).

For the purpose of MLP training and achievement evaluation, 70% (training) and 30% (testing) are divided. Sampling points are reserved using the "Random selection within subsets" function in QGIS. In the network architecture, parameters such as the number of hidden layers and neurons were determined as a result of trial and error. In addition, since the data used in the learning process of the model is in different units, it is handled equally in order to improve network performance. Therefore, the data is normalized in the 0-1 range to reduce it to a single dimension (Küçüktopcu & Cemek, 2021; Vogl et al., 1988). Matlab 2021a was used in the modeling phase of our study. Data from field and laboratory studies and remote sensing data at these points were used for MLP training.

### Model Evaluation

For the purpose of accuracy assessment of the MLP: we took into account the final output of the network and the soil moisture values that we measured in the laboratory studies. In this context, we used the error metrics we present in Table 2 to evaluate model accuracy performances.

## Results and Discussion

### Descriptive Statistics

Descriptive statistics for training, testing and all data sets are shown in Table 3. The soil moisture (SM) content measured in all dataset ranged from 1.21% to 11.48%, with a mean of 6.59% and a standard deviation (SD) of 1.71%. Soil moisture ranges from 1.10% to 7.21% in the training dataset. Test dataset soil moisture is in the range of 1.10% to 7.31%. Training and testing dataset mean is 2.82% and 3.01%, respectively. On the other hand, the standard deviations (SD) whole, training and test data sets are 1.45, 1.39, and 1.61, respectively. Training, test and all datasets have similar mean and SD values, shows that soil moisture can be successfully used in a spatial distribution model.

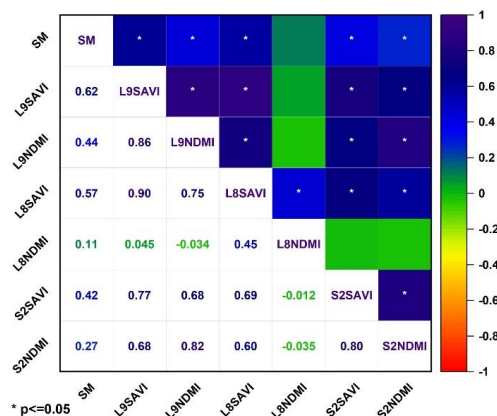


Figure 3. Correlation coefficients between independent variables and soil moisture

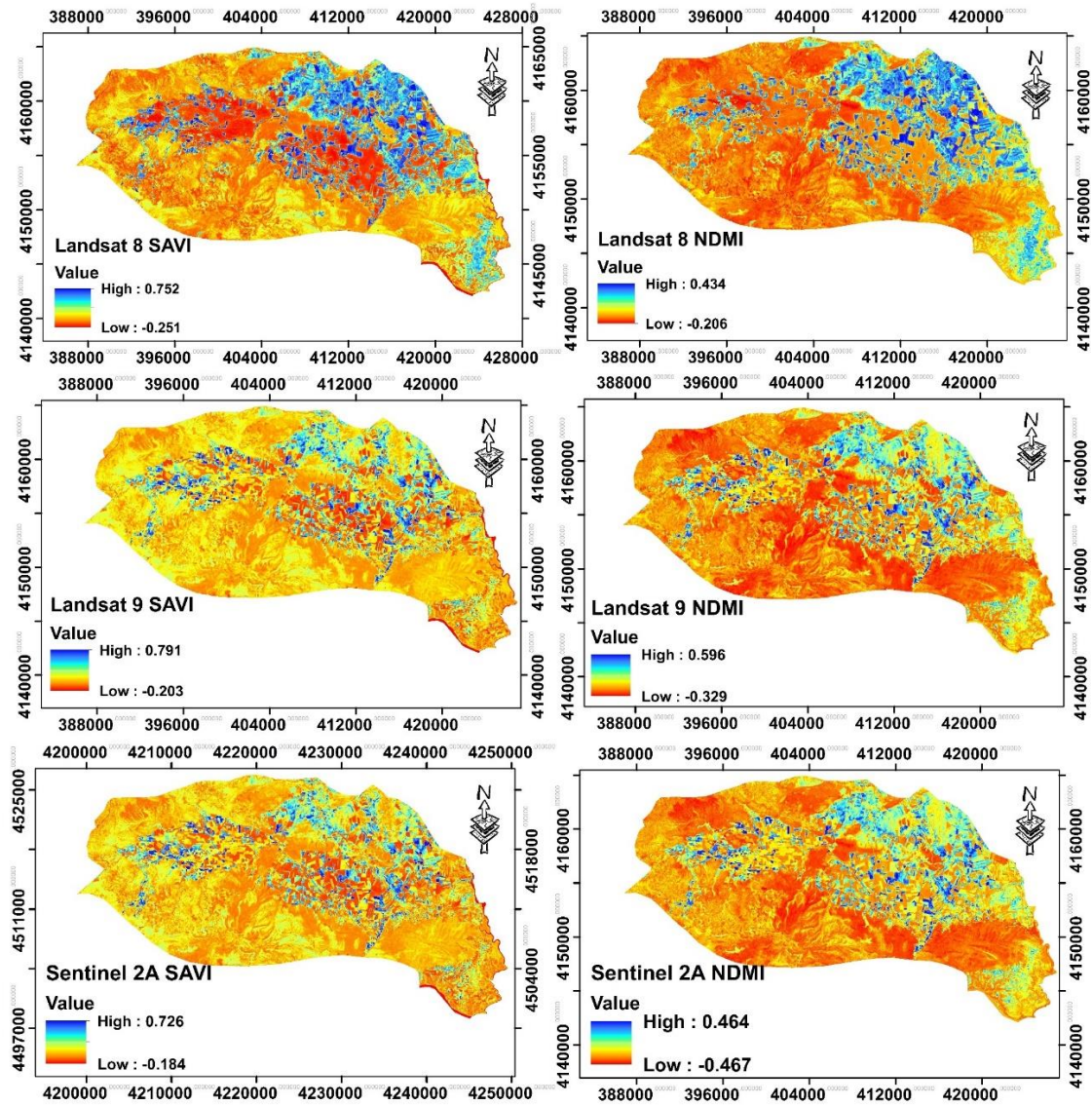


Figure 4. SAVI and NDMI maps of different optical satellite imagery

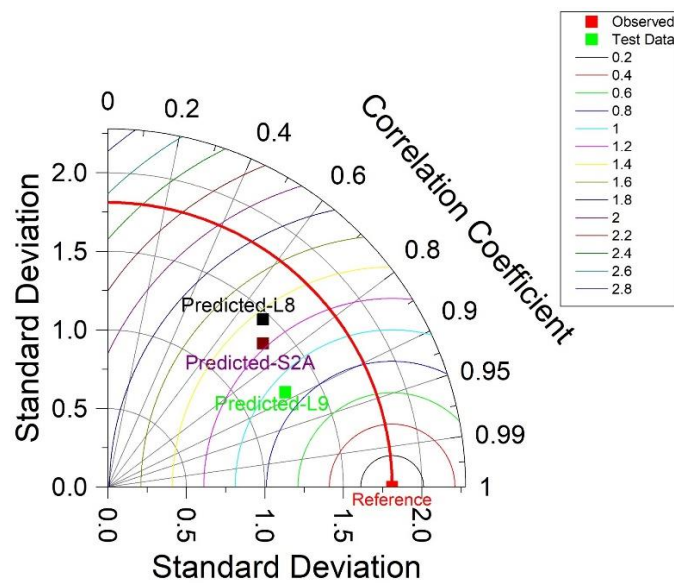


Figure 5. Illustration of Landsat 8-MLP, Landsat 9-MLP and Sentinel 2A-MLP model performances in Taylor diagram in test dataset

Pearson correlation coefficients ( $r$ ) between covariates and soil moisture content are given in Figure 3. The statistical correlation between the soil moisture content of the whole data set and the covariates with input parameters is moderate ( $P < 0.05$ ). Our results; in correspond with Fakhari-zadehshirazi et al. (2019), the vegetation index was positively correlated with soil moisture. On the other hand, Zhang ve ark. (2019); considering the spatial distribution of soil moisture with reflection data in the near infrared (NIR) and red (R) bands, have calculated the Ratio Dryness Monitoring Index (RDMI) as a new drought monitoring indicator. Showed that there was a strong negative correlation ( $r = -0.89$ ) with soil moisture content data measured at a depth of 0-10 cm. In our study, soil moisture with SAVI, which we calculated using the same bands, similarly showed a moderately strong correlation.

SAVI calculated using NIR and SWIR spectral bands of Landsat 9 (OLI-2) and Sentinel 2A MSI optical satellite images (Figure 3) and Pearson correlation coefficients between soil moisture are 0.62 and 0.42, respectively. The reason for the increased correlation between Landsat 9-SAVI and soil moisture is: It may be due to the improved of near-infrared (NIR) and shortwave infrared (SWIR) sensors with Operational Terrain Imager 2 (Masek et al., 2020). Indeed, SAVI calculated using Landsat 8 spectral bands which has an Operational Terrain Imager 1 (Figure 3) and the Pearson correlation coefficient between soil moisture is 0.57; strengthens this possibility. Because Landsat 9 OLI-2 image date is 27.05.2022 while Landsat 8 OLI image date is 26.05.2022.

Gravimetric soil moisture of Landsat 9 (OLI-2) NDMI and Sentinel 2A (MSI) NDMI and Pearson correlation coefficient, respectively 0.44 and 0.27 moderate and low levels of positive and significant relationship between were found ( $P < 0.05$ ) (Figure 3 and Figure 4). Our results; Jovanovic and ark., (2014) in their study to determine the relationship between SPOT-Vejetasyon Normalized Difference Water Index (NDWI) and measured soil moisture content, compatible with the strong relationship they achieved in the first 10 cm depth stage ( $r = 0.80$ ,  $P < 0.01$ ). Casamitjana et al. (2020) with the difference water index they calculated using the near-infrared band of the PlanetScope optical satellite image with a spatial resolution of 3 m, at the first 10 cm soil depth, they achieved a strong correlation with soil moisture, regardless of different types of land use. Our findings shows that spatial resolution, as well as radiometric improvement in optical satellite sensors, can successfully determine soil moisture. Because, Optical sensor mirror in Landsat 9 with OLI-2 healing in the near and short infrared spectral region and spectral data loss caused by scattered light reduced (Lulla et al., 2021). Also, Sentinel 2 and Landsat 9 show a similar correlation with soil moisture; Signal-to-Noise Ratio (SNR) improvement in OLI-2 may be due to improvement so for brightness 5% 1-sigma and for above-atmosphere reflection 3% (1-sigma) calibration was made. Therefore, it should be noted that the requirement for SNR performance is above Landsat 8 (OLI). Also, Between Landsat 9 and Sentinel-2 improved pixel-based geometric alignment, as seen in our study demonstrated the possibility of interoperability with Sentinel-2 (Masek et al., 2020). In this way Landsat 9 and Sentinel-2 sensors together, such as vegetation phenology identification and

agricultural yield estimation, reduce the effort to coordinate the spatial resolution gap between images for a wide range of applications, can increase the success of deep learning-based fusion algorithms with the possibility of synergistic use (Shao et al., 2019).

#### **MLP Architecture and Accuracy Assessment**

The optimal parameter results of the MLP model architecture we created for soil estimation in the upper soil layer are given in Table 4. In our study, the optimum model architecture by taking into account the RMSE value consists of 2 hidden layers. The numbers of the hidden layer node are 7-7 for Landsat 8, Landsat 9 and Sentinel 2A (Table 4).

The results of the MLP model accuracy assessment are given in Table 4. In the Sentinel 2A (MSI) test and training data set, RMSE values were 0.57 and 1.17, respectively. Similar results were obtained in the Landsat 8 (OLI) test and training datasets. Landsat 8 RMSE and MAE values were 1.16 and 0.85 in the test dataset, respectively, and 0.61 and 0.49 in the training dataset, respectively. Determination coefficient obtained as a result of forecasting and observation data regression ( $R^2$ ): test datasets were 0.53, 0.79 and 0.57 for MLP success has improved significantly in predictions made using Landsat 9. On the other hand, our Landsat 8 result is consistent with the literature J. Wang et al. (2021). Wang et al. (2021); used the Landsat 8-based Normalized Difference Water Index to obtain a soil moisture distribution map in China's Lake Ebinur Basin. He reported the results of back-propagation artificial neural network and Support Vector Regression  $R^2$  as 0.502 and 0.534, respectively.

Landsat 9 (OLI-2); High prediction success compared to Landsat 8 (OLI) and Sentinel 2A (MSI). RMSE is 0.79 in Landsat 9 (OLI-2) test dataset while 0.53 in training dataset. MAE value is 0.66 and 0.42 in the test and training dataset, respectively. MLP is an algorithm that performs predictions with a data-driven approach. Therefore, data quality has a significant impact on network prediction success (Khaledian & Miller, 2020; Schmidhuber, 2015). As Masek et al. (2020) point out; The effect of corrections made to Landsat 9 (OLI 2) NIR and SWIR sensors on improving data quality is a possible reason for the success seen in the estimate results.

Taylor diagram is a good way to visualize the prediction performance of different models visually in 2D (Denis et al., 2003). According to Taylor diagram (Figure 5), The Landsat 9-MLP model is closer to the Reference point, represented in red, making it more successful than the Landsat 8-MLP and Sentinel 2A-MLP. Landsat 9-MLP model prediction results showed a highly correlated correlation with the observed values, taking place in the 0.9-0.95 ( $r$ ) sector. The Landsat 8-MLP and Sentinel 2A-MLP models are available in the 0.8-0.9 ( $r$ ) sector. Centered Root Mean Square Error (CRMSE), centered according to reference values, is represented by semicircles represented by different colours (Figure 5). The CRMSE value of Landsat 9-MLP is close to 0.8 sector, represented by purple. The Taylor diagram results confirm that Landsat 9-MLP model prediction success is higher than Landsat 8-MLP and Sentinel 2A-MLP.

## Conclusion

In this study SAVI and NDMI, Landsat 9 (OLI-2), Landsat 8 (OLI) and Sentinel 2A (MSI) which are the most commonly used radiometric indices in soil moisture estimation, were calculated using optical satellite images. The latest member of the NASA-USGS joint mission is Landsat 9, improvements made with Operational Land Imager 2 (OLI-2) for multispectral imaging at near- and short-wave infrared wavelengths, the effect on MLP model performance, which is widely used in digital soil mapping, was tried to be revealed. Landsat 9 (OLI-2) based SAVI and NDMI showed a moderately significant positive correlation relationship with gravimetric soil moisture. The correlation relationship between Landsat 8 (OLI) and Sentinel 2A (MSI) based radiometric indices and soil moisture was lower than Landsat 9 (OLI-2). This case is the result of the improvement in radiometric data quality as a result of the improvement in the optical sensor mirror and the reduced signal-to-noise ratio in the near and short infrared spectral region of Landsat 9 (OLI-2). Improved data quality positively impacted MLP network prediction performance. Landsat 9-MLP forecasting success increased significantly compared to Landsat 8-MLP and Sentinel 2-MLP. Our results suggest that Landsat 9 (OLI-2) can be reliably used in soil moisture spatial forecasting models. In future studies, Landsat 9 and Sentinel-2 sensors with fusion images obtained with common synergy, the forecasting success of artificial intelligence algorithms used in digital soil mapping applications should be increased.

## Declaration of Competing Interest

The authors declare no conflict of interest.

## References

- Abowarda AS, Bai L, Zhang C, Long D, Li X, Huang Q, Sun Z. 2021. Generating surface soil moisture at 30 m spatial resolution using both data fusion and machine learning toward better water resources management at the field scale. *Remote Sensing of Environment*, 255: 112301. <https://doi.org/10.1016/j.rse.2021.112301>
- Amani M, Parsian S, MirMazloumi SM, Aienh O. 2016. Two new soil moisture indices based on the NIR-red triangle space of Landsat-8 data. *International Journal of Applied Earth Observation and Geoinformation*, 50: 176–186. <https://doi.org/10.1016/j.jag.2016.03.018>
- Babaeian E, Sidike P, Newcomb MS, Maimaitijiang M, White S. A, Demieville J, Ward RW, Sadeghi M, LeBauer DS, Jones SB, Sagan V, Tuller M. 2019. A New Optical Remote Sensing Technique for High-Resolution Mapping of Soil Moisture. *Frontiers in Big Data*, 2. <https://doi.org/10.3389/fdata.2019.00037>
- Bidgoli RD, Koohbanani H, Keshavarzi A, Kumar V. 2020. Measurement and zonation of soil surface moisture in arid and semi-arid regions using Landsat 8 images. *Arabian Journal of Geosciences*, 13(17): 826. <https://doi.org/10.1007/s12517-020-05837-2>
- Carlson T. 2007. An Overview of the “Triangle Method” for Estimating Surface Evapotranspiration and Soil Moisture from Satellite Imagery. *Sensors*, 7(8): 1612–1629. <https://doi.org/10.3390/s7081612>
- Casamitjana M, Torres-Madroño MC, Bernal-Riobo J, Varga, D. (2020). Soil Moisture Analysis by Means of Multispectral Images According to Land Use and Spatial Resolution on Andosols in the Colombian Andes. *Applied Sciences*, 10(16): 5540. <https://doi.org/10.3390/app10165540>
- Cerasoli S, Campagnolo M, Faria J, Nogueira C, Caldeira Mda C. (2018). On estimating the gross primary productivity of Mediterranean grasslands under different fertilization regimes using vegetation indices and hyperspectral reflectance. *Biogeosciences*, 15(17): 5455–5471. <https://doi.org/10.5194/bg-15-5455-2018>
- Chaudhary SK, Srivastava PK, Gupta DK, Kumar P, Prasad R, Pandey DK, Das AK, Gupta M. 2022. Machine learning algorithms for soil moisture estimation using Sentinel-1: Model development and implementation. *Advances in Space Research*, 69(4): 1799–1812. <https://doi.org/10.1016/j.asr.2021.08.022>
- Congedo L. 2021. Semi-Automatic Classification Plugin Documentation (Release 7.).
- Dai F, Zhou Q, Lv Z, Wang X, Liu G. 2014. Spatial prediction of soil organic matter content integrating artificial neural network and ordinary kriging in Tibetan Plateau. *Ecological Indicators*, 45: 184–194. <https://doi.org/10.1016/j.ecolind.2014.04.003>
- Das AC, Noguchi R, Ahamed T. 2021. An Assessment of Drought Stress in Tea Estates Using Optical and Thermal Remote Sensing. *Remote Sensing*, 13(14): 2730. <https://doi.org/10.3390/rs13142730>
- Denis B, Laprise R, Caya D. 2003. Sensitivity of a regional climate model to the resolution of the lateral boundary conditions. *Climate Dynamics*, 20(2): 107–126. <https://doi.org/10.1007/s00382-002-0264-6>
- Fakharizadehshirazi E, Sabziparvar AA, Sodoudi S. 2019. Long-term spatiotemporal variations in satellite-based soil moisture and vegetation indices over Iran. *Environmental Earth Sciences*, 78(12): 342. <https://doi.org/10.1007/s12665-019-8347-4>
- Huete A. 1988. A soil-adjusted vegetation index (SAVI). *Remote Sensing of Environment*, 25(3): 295–309. [https://doi.org/10.1016/0034-4257\(88\)90106-X](https://doi.org/10.1016/0034-4257(88)90106-X)
- Isaaks H, Mohan R. 1989. An Introduction to Applied Geostatistics. In Oxford University Press. [https://doi.org/https://doi.org/10.1016/0098-3004\(91\)90055-I](https://doi.org/https://doi.org/10.1016/0098-3004(91)90055-I)
- Jovanovic N, Garcia C, Bugan R, Teich I, Rodriguez C. 2014. Validation of remotely-sensed evapotranspiration and NDWI using ground measurements at Riverlands, South Africa. *Water SA*, 40(2): 211. <https://doi.org/10.4314/wsa.v40i2.3>
- Khaledian Y, Miller BA. 2020. Selecting appropriate machine learning methods for digital soil mapping. *Applied Mathematical Modelling*, 81: 401–418. <https://doi.org/https://doi.org/10.1016/j.apm.2019.12.016>
- Khorrarn S, Nelson SAC, Koch FH, van der Wiele CF. 2012. *Remote Sensing*. Springer US. <https://doi.org/10.1007/978-1-4614-3103-9>
- Kraft B, Jung M, Körner M, Koirala S, Reichstein M. 2022. Towards hybrid modeling of the global hydrological cycle. *Hydrology and Earth System Sciences*, 26(6): 1579–1614. <https://doi.org/10.5194/hess-26-1579-2022>
- Küçüktopcu E, Cemek B. 2021. The use of artificial neural networks to estimate optimum insulation thickness, energy savings, and carbon dioxide emissions. *Environmental Progress and Sustainable Energy*, 40(1). <https://doi.org/10.1002/ep.13478>
- Lloret J, Sendra S, Garcia L, Jimenez JM. 2021. A Wireless Sensor Network Deployment for Soil Moisture Monitoring in Precision Agriculture. *Sensors*, 21(21): 7243. <https://doi.org/10.3390/s21217243>
- Lulla K, Nellis MD, Rundquist B, Srivastava PK, Szabo S. 2021. Mission to earth: LANDSAT 9 will continue to view the world. *Geocarto International*, 36(20): 2261–2263. <https://doi.org/10.1080/10106049.2021.1991634>
- Masek JG, Wulder A, Markham B, McCorkel J, Crawford CJ, Storey J, Jenstrom DT. 2020. Landsat 9: Empowering open science and applications through continuity. *Remote Sensing of Environment*, 248: 111968. <https://doi.org/10.1016/j.rse.2020.111968>

- Mevbis, 2022. Meteorolojik Veri Bilgi Sunum ve Satış Sistemi. <https://mevbis.mgm.gov.tr/mevbis/ui/index.html#/Workspace>
- Mukwada G, Mazibuko SM, Moeletsi M, Robinson GM. 2021. Can Famine Be Averted? A Spatiotemporal Assessment of The Impact of Climate Change on Food Security in The Luvuvhu River Catchment of South Africa. *Land*, 10(5): 527. <https://doi.org/10.3390/land10050527>
- O'Connell CS, Ruan L, Silver WL. 2018. Drought drives rapid shifts in tropical rainforest soil biogeochemistry and greenhouse gas emissions. *Nature Communications*, 9(1): 1348. <https://doi.org/10.1038/s41467-018-03352-3>
- Oliveira VA, Rodrigues AF, Morais MAV, Terra M, De CNS, Guo L, Mello CR. 2021. Spatiotemporal modelling of soil moisture in an <sc>A</sc> tantic forest through machine learning algorithms. *European Journal of Soil Science*, 72(5): 1969–1987. <https://doi.org/10.1111/ejss.13123>
- Ortaç Y. 2020. Besni (Adıyaman) İlçesinin Beşerî ve Ekonomik Coğrafyası. Kahramanmaraş Sütçü İmam Üniversitesi.
- Pittaki-Chrysodonta Z, Moldrup P, Knadel M, Iversen BV, Hermansen C, Greve MH, De Jonge LW. 2018. Predicting the Campbell Soil Water Retention Function: Comparing Visible-Near-Infrared Spectroscopy with Classical Pedotransfer Function. *Vadose Zone Journal*, 17(1): 170169. <https://doi.org/10.2136/vzj2017.09.0169>
- Sadri S, Pan M, Wada Y, Vergopolan N, Sheffield J, Famiglietti JS, Kerr Y, Wood E. 2020. A global near-real-time soil moisture index monitor for food security using integrated SMOS and SMAP. *Remote Sensing of Environment*, 246: 111864. <https://doi.org/10.1016/j.rse.2020.111864>
- Schmidhuber J. 2015. Deep learning in neural networks: An overview. *Neural Networks*, 61: 85–117. <https://doi.org/https://doi.org/10.1016/j.neunet.2014.09.003>
- Senel G. 2018. Delineation of Water Bodies with Landsat 8 and Sentinel 2 Satellite Imagery Using Different Image Processing Algorithms.
- Sergeev AP, Buevich AG, Baglaeva EM, Shichkin AV. 2019. Combining spatial autocorrelation with machine learning increases prediction accuracy of soil heavy metals. *CATENA*, 174: 425–435. <https://doi.org/https://doi.org/10.1016/j.catena.2018.11.037>
- Somaratne S, Seneviratne G, Coomaraswamy U. 2005. Prediction of Soil Organic Carbon across Different Land-use Patterns. *Soil Science Society of America Journal*, 69(5): 1580–1589. <https://doi.org/10.2136/sssaj2003.0293>
- Tüzüner A. 1990. Toprak ve Su Analiz Laboratuvarları El Kitabı. Tarım Orman ve Köyişleri Bakanlığı.
- USGS, 2013. Landsat 8: U.S. Geological Survey Fact Sheet. <https://pubs.usgs.gov/fs/2013/3060/pdf/fs2013-3060.pdf>
- USGS, 2019. Landsat 9 fact sheet. <https://www.usgs.gov/media/images/landsat-9-fact-sheet>
- Vogl TP, Mangis JK, Rigler AK, Zink WT, Alkon DL. 1988. Accelerating the convergence of the back-propagation method. *Biological Cybernetics*, 59(4): 257–263. <https://doi.org/10.1007/BF00332914>
- Wang H. 2019. Soil Moisture Retrieval from Microwave Remote Sensing Observations. In *Soil Moisture*. IntechOpen. <https://doi.org/10.5772/intechopen.81476>
- Wang J, Wang W, Hu Y, Tian S, Liu D. 2021. Soil Moisture and Salinity Inversion Based on New Remote Sensing Index and Neural Network at a Salina-Alkaline Wetland. *Water*, 13(19): 2762. <https://doi.org/10.3390/w13192762>
- Wang L, Qu JJ. 2009. Satellite remote sensing applications for surface soil moisture monitoring: A review. *Frontiers of Earth Science in China*, 3(2): 237–247. <https://doi.org/10.1007/s11707-009-0023-7>
- Yıldırım Y. 2004. Kuruluş yeri bakımından Besni ilçe merkezi (Adıyaman) ve çevresinin jeomorfolojisi. Fırat Üniversitesi.
- Zhang J, Zhang Q, Bao A, Wang Y. 2019. A New Remote Sensing Dryness Index Based on the Near-Infrared and Red Spectral Space. *Remote Sensing*, 11(4): 456. <https://doi.org/10.3390/rs11040456>
- Zounemat-Kermani M, Golestani Kermani S, Alizamir M, Fadaee M. 2022. Soil moisture simulation using individual versus ensemble soft computing models. *International Journal of Environmental Science and Technology*. <https://doi.org/10.1007/s13762-022-04202-y>